Spatiotemporally periodic states, periodic windows, and intermittency in coupled-map lattices

Qu zhilin
Department of Physics, Beijing Normal University, Beijing 100875, China

Hu Gang
Center of Theoretical Physics, Chinese Center of Advanced Science and Technology (World Laboratory), Beijing, P.O. Box 8730, China;
Department of Physics, Beijing Normal University, Beijing 100875, China;
and Institute of Theoretical Physics, Academia Sinica, Beijing, China

(Received 6 July 1993)

Several stable spatiotemporally periodic states in coupled- (logistic) map lattices are analytically obtained. Spatiotemporally periodic windows are found in the parameter region where the single logistic map is in a fully developed chaotic state. Spatiotemporal intermittency transients and spatiotemporal intermittency and their mechanisms are discussed. Chaotic supertransients and their average transient lengths are investigated. The influence of the system size on the system dynamics is analyzed numerically in detail. Finally, we try to control chaotic supertransients by pinnings; the astronomically long transients are impressively shortened after controlling.

PACS number(s): 05.45.+b, 47.20.Ky

I. INTRODUCTION

Turbulence exists extensively in nature, such as in fluids, optics, chemical reactions, plasma, and biology systems, etc. It is very important to characterize these spatiotemporal complexities both theoretically and experimentally. The high dimensionality of the space-time systems causes many difficulties both in analytical and numerical studies. Coupled-map lattices (CML's) [1–23] are the most convenient tools in this investigation. In this paper, we focus our attention on the model of a one-dimensional CML.

A CML is a dynamical system with a discrete time, discrete space, and continuous state. The widely studied one-dimensional model has the following form:

$$x_{n+1}(i)=(1-\epsilon)f(x_n(i))+\sum_{\substack{j=-k\\ j\neq 0}}^{k}\beta_j f(x_n(i-j)) , \tag{1}$$

with

$$\sum_{\substack{j=-k\\ j\neq 0}}^{k}\beta_j=\epsilon , \tag{2}$$

where n is the discrete time step, i the lattice site label, and β_j the diffusion constants. The simplest model with symmetrical couplings is the nearest-neighbor coupled diffusive model ($\beta_{-1}=\beta_1=\epsilon/2$) [2–6,19–22]:

$$x_{n+1}(i)=(1-\epsilon)f(x_n(i))+\frac{\epsilon}{2}\{f(x_n(i-1))+f(x_n(i+1))\} . \tag{3}$$

In this presentation, we restrict ourselves in this case. Here we assume a periodic boundary condition, $x_n(i)=x_n(i+L)$, with L being the system size. The initial conditions are prepared, unless specified otherwise, to be the random numbers ranging from 0 to 1 in most of our calculations. The mapping function $f(x)$ is chosen to be the logistic map:

$$f(x)=ax(1-x) , \tag{4}$$

which shows periodic doubling at $a=3$ with the accumulation point at $a=a_c=3.569\ldots$. This map is either periodic or chaotic when $a>a_c$, and for $a=4$, $f(x)$ maps the interval [0,1] exactly into itself, and the dynamics are in a fully developed chaotic state. In this paper, we investigate the case of $a=4$ in most of our discussions.

Many results on CML's have been published; for instance, Kaneko and co-worker [1–6] have investigated the statistical properties, pattern selections, supertransient, spatiotemporal intermittency (STI), spatiotemporal intermittency transient (STIT), etc.; Keeler and Farmer [10] and Chate and Manneville [11] have studied in detail the STI, while Bohr and co-workers [7–9] and other authors [12–22] have investigated the correlation length, Lyapunov exponents, soliton waves, phase transitions, and so on. In this paper, we first discuss the low-dimensional stable periodic attractors of Eq. (3) and their extension to high-dimensional cases (Sec. II). *Spatiotemporally periodic windows* (SPW's) are shown here in CML systems. In Sec. III we investigate a class of STIT and STI in CML's, and some explanations are given for the mechanism of this kind of STIT and STI. In Sec. IV, we will study the supertransients of those stable attractors discussed in Sec. II. Finally, we try to control the chaotic supertransients by pinning feedbacks to the lattice sites to shorten the astronomically long transients of the system in Sec. V.

II. SPATIOTEMPORALLY PERIODIC STATES AND PERIODIC WINDOWS IN CML'S

A. Low-dimensional stable attractors

To investigate the behaviors of high-dimensional systems, it is sometimes very useful first to look at the low-dimensional ones, especially for Eq. (3) due to its high symmetry. First we take $L=2$, and reduce Eq. (3) to

$$\begin{aligned} x_{n+1}(1)&=(1-\epsilon)f(x_n(1))+\epsilon f(x_n(2)) ,\\ x_{n+1}(2)&=(1-\epsilon)f(x_n(2))+\epsilon f(x_n(1)) . \end{aligned} \tag{5}$$

An inhomogeneous fixed-point solution (we will denote temporal period-m states as Tm, spatial period-k states as Sk; thus this fixed-point solution is denoted as T1S2) can be analytically worked out as

$$x_{\pm}=\frac{(1-a+2a\epsilon)\pm\sqrt{(1-a+2a\epsilon)^2-4(\epsilon-a\epsilon+2a\epsilon^2)}}{2a(2\epsilon-1)} . \tag{6}$$

This state exists when

$$a>2+\frac{1}{2\epsilon-1} . \tag{7}$$

The minimum a for this state is $a_{\min}=3$, which is just the parameter point of periodic doubling. Linear stability analysis shows the following maximum Lyapunov exponent (λ):

$$\lambda=\ln\left|-\frac{1-\epsilon}{2\epsilon-1}-\left[\frac{(3\epsilon-1)^2}{(2\epsilon-1)^2}+(2\epsilon-1)a(2-a)\right]^{1/2}\right| . \tag{8}$$

And the stability boundary in ϵ-a space can be easily obtained from Eq. (8):

$$\epsilon_-=\frac{1+\sqrt{3/a(a-2)}}{2} , \quad \epsilon_+=\frac{3+2a(a-2)+\sqrt{[3+2a(a-2)]^2-4a(a-2)(a-1)^2}}{4a(a-2)} . \tag{9}$$

At ϵ_- the maximum eigenvalue is a negative unit, while at ϵ_+ the eigenvalues are a pair of conjugate numbers with unit modulus; thus period doubling occurs at ϵ_- and Hopf bifurcation at ϵ_+.

From (5) and (6) we can easily deduce that there exists an antiphase T2S2 state. Inserting Eq. (6) into Eq. (5) after substituting ϵ by $1-\epsilon$ in Eqs. (5) and (6), we arrive at

$$\begin{aligned} x_+&=(1-\epsilon)f(x_-)+\epsilon f(x_+) ,\\ x_-&=(1-\epsilon)f(x_+)+\epsilon f(x_-) . \end{aligned} \tag{10}$$

Obviously, it is just an antiphase T2S2 state (x_-x_+, x_+x_-), and the simple transformation indicates that if there exists a T1S2 state at ϵ_0 there must be an antiphase T2S2 state at $1-\epsilon_0$. For the linear stability analysis, we need only substitute ϵ by $1-\epsilon$ in Eq. (8) to obtain the maximum Lyapunov exponent of the T2S2 state. The bifurcation at $(1-\epsilon_-)$ is tangent other than period doubling and at $(1-\epsilon_+)$ is Hopf.

Furthermore, an antiphase T2S4 state ($x_-x_+x_+x_-$, $x_+x_-x_-x_+$) can also be easily deduced from the antiphase T2S2 state: Because $x_n(i+1)=x_n(i-1)$ for the T2S2 state, then Eq. (3) for the T2S2 state is reduced to

$$x_{n+1}(i)=(1-\epsilon)f(x_n(i))+\epsilon f(x_n(i+1)) , \tag{11}$$

while for the T2S4 state $x_n(i+1)\neq x_n(i-1)$, we have instead either $x_n(i+1)=x_n(i)$ or $x_n(i-1)=x_n(i)$. Let $x_n(i-1)=x_n(i)$ [the analysis is the same for $x_n(i+1)=x_n(i)$], Eq. (3) can be reduced to

$$x_{n+1}(i)=\left[1-\frac{\epsilon}{2}\right]f(x_n(i))+\frac{\epsilon}{2}f(x_n(i+1)) . \tag{12}$$

Comparing Eq. (11) with Eq. (12), one finds at once that the difference between the two equations is only the factor $\frac{1}{2}$. Thus, if there exists a T2S2 state at ϵ_0, there must be a T2S4 state at $2\epsilon_0$. Generally, if there exists a TmS2 state at ϵ_0 there must be a TmS4 state at $2\epsilon_0$, for any time period m. With some algebra, we can verify that we just need to substitute ϵ by $(1-\epsilon)/2$ in Eq. (8) to obtain the maximum Lyapunov exponent of the T2S4 state. The bi-

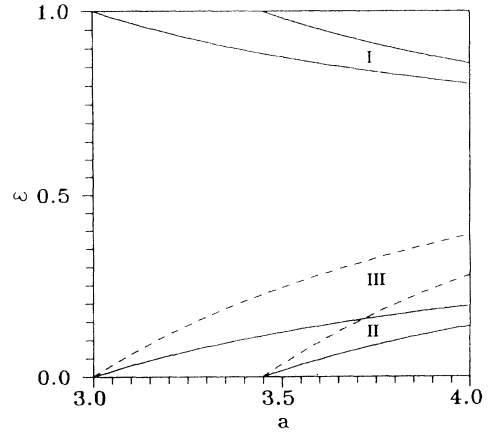

FIG. 1. The stability boundaries for T1S2 (I, $L=2$), T2S2 (II, $L=2$), and T2S4 (III, $L=4$) states in ϵ-a space.

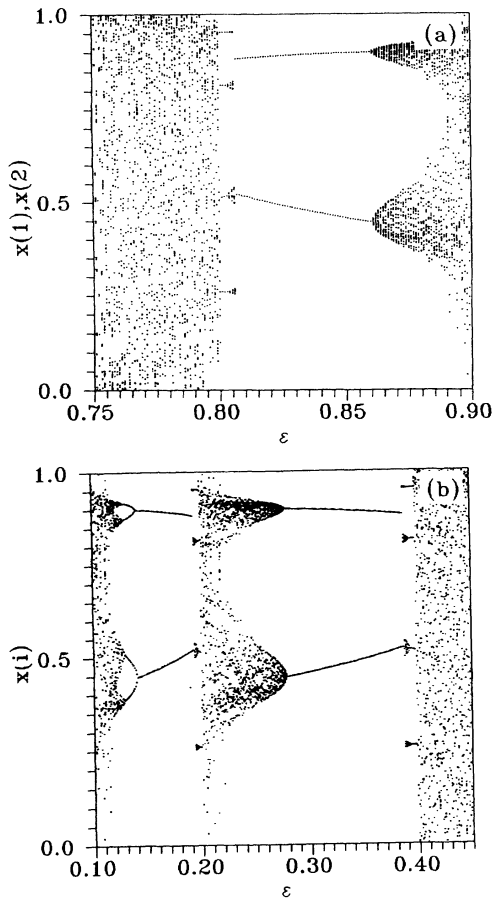

FIG. 2. Bifurcations of the system versus diffusion constant ϵ for $L=4$ and $a=4$. (a) Chaos→T4S2→T1S2→chaos; (b) Chaos→T4S4→T2S2→T4S2→chaos→T2S4→T4S4→chaos.

furcation behaviors of the T2S4 state are just like those of the T2S2 state. Therefore, we have obtained three kinds of periodic states analytically, with the stability boundaries being (Fig. 1)

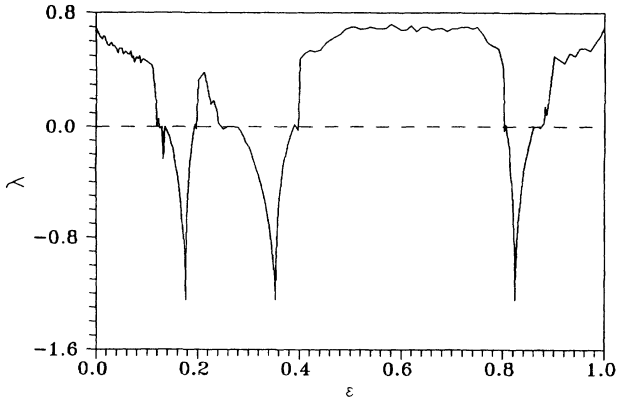

FIG. 3. λ versus ϵ for $L=4$. The similarity of the three regions is clearly seen.

$$\begin{aligned}&[\epsilon_-,\epsilon_+] \text{ for the T1S2 state},\\ &[1-\epsilon_+,1-\epsilon_-] \text{ for the T2S2 state},\\ &[2(1-\epsilon_+),2(1-\epsilon_-)] \text{ for the T2S4 state},\end{aligned} \tag{13}$$

where ϵ_- and ϵ_+ are specified in Eq. (9).

Actually, the existence of the T1S2 and T2S2 states has been reported in Refs. [19], [21], and [22], but the T2S4 state is reported here for the first time because the solution cannot be obtained so directly. In Fig. 2 we show the bifurcations of Eq. (3) versus ϵ for $a=4$ and $L=4$. Besides the T1 and T2 states analytically obtained above, there are some T4 states bifurcated from the T1 and T2 states. Figure 3 plots the maximum Lyapunov exponents (λ) for $a=4$ and $L=4$ by varying ϵ. The similarity of the three stable regions is clearly seen.

Besides the three analytical solutions obtained in Eqs. (9)–(12), we can also analytically obtain an antiphase T2S6 state $(x_1x_2x_2x_1x_3x_3,x_1x_3x_3x_1x_2x_2)$, with x_1,x_2,x_3 being

$$\begin{aligned}x_1&=\frac{(2-3\epsilon)a+\epsilon-2+\left\{[(2-3\epsilon)a+\epsilon-2]^2+\frac{4(2-3\epsilon)[(2-\epsilon)a+2]\epsilon}{2-\epsilon}\right\}^{1/2}}{2(2-3\epsilon)a},\\ x_{2,3}&=\frac{\left[1-\frac{\epsilon}{2}\right]a+1\pm\left\{\left[\left[1-\frac{\epsilon}{2}\right]a+1\right]^2-(2-\epsilon)a\left[2+\frac{4}{(2-\epsilon)a}-\epsilon f(x_1)\right]\right\}^{1/2}}{(2-\epsilon)a}.\end{aligned} \tag{14}$$

This state is stable at $a=4$ for $0.55<\epsilon<1$. Numerical simulations reveal that solution (14) is not the unique stable T2S6 state in the region of $0.64<\epsilon<0.69$, and that there are several other stable T2S6 states which finally go back to the solution (14) as $\epsilon<0.64$ and $\epsilon>0.69$.

By numerical simulations we find many other stable attractors in the region ($a=4$) where the single logistic map is in fully developed chaos. For instance, there is a stable S5 state for $\epsilon=0.36$ to 0.58, a stable S7 state for $\epsilon=0.56$ to 1, etc. In Fig. 4 we show a number of the spatially periodic stable states in the CML at $a=4$. Three points are worthwhile remarking about at this stage.

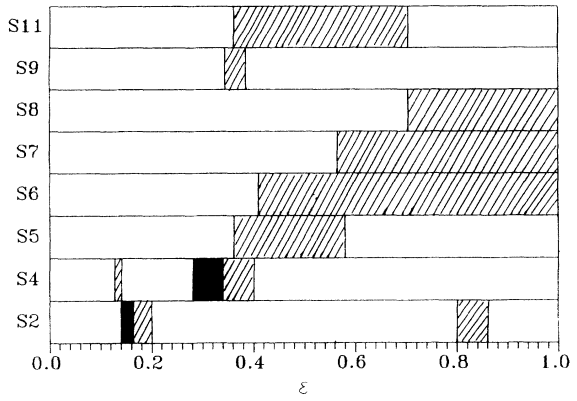

FIG. 4. The stability boundaries of several spatially periodic states for $a=4$. The stable regions of these states are shaded, while the SPW's are blackened. For shaded regions we take $L=k$ for Sk, $k=2,4,5,\ldots$, while for SPW, we mean that for $L=mk$, $k=2$ and 4, $m=1,2,3,\ldots$, the system has a unique attractor for the given parameters (Sec. II B).

First, it is interesting to point out that the previous works have shown that at $a=4$ the diffusion region of $\epsilon>0.2$ is a fully developed turbulence region for the CML's [4]. However, here we find that in the well-known fully developed turbulence region and stable attractors are still very "dense" (Fig. 4). Second, the existence of such stable periodic attractors strongly depends on the lattice sizes of the system. Thus, the influence of system sizes on the spatiotemporal structures is a crucial point in the study of CML. Third, though we find a great number of stable periodic structures in the CML system at a fully developed chaos region ($a=4$, $\epsilon>0.2$), the systematic bifurcation sequences, such as periodic doubling both spatially and temporally, leading to chaos have not been found, which is not like the case at the accumulating point [22]. Chaos often bursts abruptly via intermittency or crises.

B. Spatiotemporally periodic windows in coupled-map lattice

In Sec. II A we discussed the low-dimensional stable periodic states in the CML's. The problems of apparent significance are whether the stable periodic states found in low-dimensional cases are still stable for larger L and how the attracting basins depend on the system size if the periodic states remain stable. The stability of the spatially periodic states in CML's has been analytically discussed in Refs. [21] and [22], which reveal that the stability boundary of a spatially periodic state may be changed by changing the system size L. For example, the lower boundary of the T2S2 state slightly shifts from $\epsilon=0.1392\ldots$ to $\epsilon=0.14037\ldots$ at $a=4$ as L goes to infinity [21]. Here we only use numerical simulations to test the stability of the periodic states mentioned in Sec. II A for large L. In a certain parameter region there is a unique stable state. We call such a parameter region *spatiotemporally periodic window* (SPW).

In Fig. 5 we show the λ's of the system versus L for $\epsilon=0.15$, 0.3, and 0.6 at $a=4$. A comparison of Fig. 5 with the results obtained by Bohr and co-workers [8,9] is interesting. In Refs. [8] and [9] the authors mainly investigated the λ's not far from the accumulating point. The size dependence of the λ's is the following. The λ's are first equal to that of the single map for small L, and after certain critical system sizes the λ suddenly drops to zero and is maintained at zero until the second critical size, after which all the λ's are maintained approximately to a half of that of the single map (see Fig. 1 in Ref. [8]). Fig-

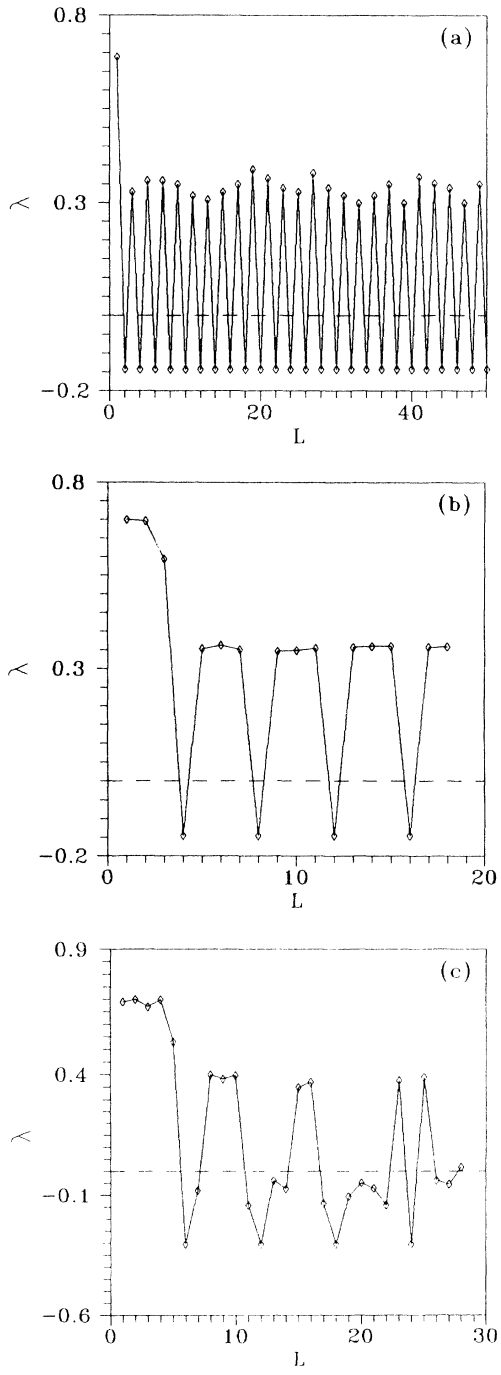

FIG. 5. λ versus L at $a=4$. (a) $\epsilon=0.15$; (b) $\epsilon=0.3$; (c) $\epsilon=0.6$.

ure 5(a) shows the λ's of the system versus L at $\epsilon=0.15$ and $a=4$. For $L=2,4,6,\ldots$, the λ's are negative with the same value, which means that the system finds the same attractor (T2S2), while for odd L's the λ's are positive, which is dramatically different from the picture in Ref. [8]. Figure 5(b) shows the case for $\epsilon=0.3$. The first two λ's are equal to ln2, which means that the system is in the homogeneous chaotic state at $L=2$. At $L=4k$ ($k=1,2,3,\ldots$) the λ's take the same negative value and thus the system finds the same attractor (T2S4), while at $L\neq 4k$ the λ's are positive. At $\epsilon=0.6$ [Fig. 5(c)], the λ's versus L are not so regular, due to the coexistence of many stable attractors. But the essential features are not changed. For example, at $L=6,12,18,24$, the λ's are negative with the same value and thus the system finds the same stable attractor (T2S6), though the initial conditions are changed. The above three cases have a common feature in that after the system first finds the stable attractor by increasing L, the λ's of chaotic attractors are maintained to about $\frac{1}{2}\ln 2$. This well confirms the arguments in Refs. [8] and [9], though our parameters are taken in the fully developed turbulence region.

Figures 6(a)–6(c) show the space-time structures of the stable attractors for $L=60$, and $\epsilon=0.15$, 0.3, and 0.6, respectively. However, it is almost impossible to reach the stable states for such long chains at $\epsilon=0.3$ and 0.6 with completely random initial conditions due to the extremely long transients. But if we prepare the initial conditions as $x_0(i)=\bar{x}(i)+\sigma\xi(i)$ [$\bar{x}(i)$ is a solution of the stable state, σ a small constant, and $\xi(i)$ random numbers ranging from -1 to 1], we can find that the system quickly approaches the stable attractors for σ sufficiently small for any system sizes that indicate the existence of the stable attractors. Thus these three attractors are at least locally stable. We have roughly estimated the maximum σ for the attractors for which there are no chaotic bursts for any initial preparations of $\xi(i)$. For the T2S2 state at $\epsilon=0.15$ and the T2S4 state at $\epsilon=0.3$, we find $\sigma_{\max}=0.04$ as the system sizes expand to very large values (e.g., $L=3000$). We define here $\sigma_{\max}$ as the "basin width" and $\sigma^{L}_{\max}$ as the "basin volume" of a stable attractor for system size L. It is interesting to point out that the basin widths of the T2S2 and T2S4 states have no observable changes as L increases, while the basin width of the T2S6 state decreases quickly as L increases.

We find in the ϵ-a space that there are some regions where the stable attractors are unique. For example, at $\epsilon=0.15$ and $a=4$, we tried many different initial conditions and different system sizes, the system always arrested by the T2S2 state for even L but in turbulence for odd L (Fig. 5). By numerical check, we find, for $0.14\ldots<\epsilon<0.163\ldots$ and $0.28\ldots<\epsilon<0.34\ldots$ at $a=4$, the stable attractors are uniquely T2S2 and T2S4 states, respectively. These two regions can extend to smaller a regions, and we call these two parameter regions in ϵ-a space SPW's of CML's. At $a=4$ and $0.163\ldots<\epsilon<0.1938\ldots$, there coexist many stable attractors of which the existence does not depend on system sizes chosen and thus pattern selections are common. In Fig. 6(d) we show one of the patterns for $\epsilon=0.18$ and $L=60$, which is dominated by the T2S2 state, while

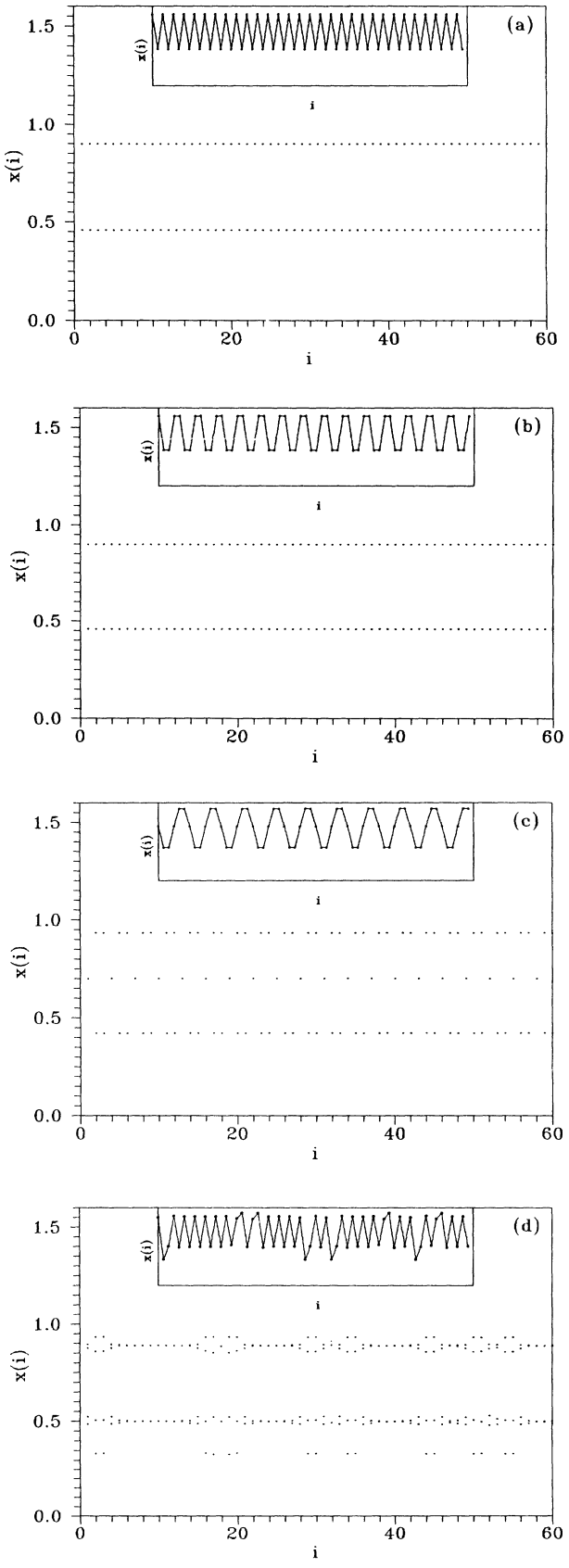

FIG. 6. The time-space structures of the stable states for $L=60$ and $a=4$; the snapshots of the stable states are plotted in the small frames. (a) $\epsilon=0.15$; (b) $\epsilon=0.3$; (c) $\epsilon=0.6$; (d) $\epsilon=0.18$.

several T4 domains appear, and the patterns selected in this parameter region are very sensitive to the initial conditions chosen.

III. STI AND STIT

Weak turbulence can take the form of STI, i.e., a sustained regime where coherent-regular and disordered-chaotic domains coexist and evolve in time and space. Although STI is observed widely in physical systems—for instance, laboratory examples can be found in Rayleigh-Bénard convection [24,25]—there are few theories for it. It is known that there are three types of temporal intermittency, described by Pomeau and Manneville [26], Grebogi, Ott, and Yorke [27], and Cruthfield [28]. Keeler and Farmer have investigated a class of STI in detail and explained them by both the Pomeau-Manneville and the Cruthfield theories [10].

In this section we will be involved in the STI and STIT in our one-dimensional CML model. As we have discussed before, there are SPW's in the turbulence region, where the attractors are unique. For instance, we always encounter the same stable zigzag pattern (T2S2 state) at $\epsilon=0.15$ and $a=4$ of any even system size L, and turbulence for odd L. By numerical simulations we find STIT for even L and robust STI for odd L. In Fig. 7(a) we show the STIT for $\epsilon=0.15$ and $L=60$. After about 14 000 iterations, the STIT disappears and the system is finally arrested by the stable T2S2 attractor. Figure 7(b) shows the STI for $\epsilon=0.15$ and $L=59$, while Fig. 7(c) shows its spatiotemporal structure in the time interval of $n=10\,000$ to 10 050. The STIT and STI shown in the figures are rather impressive. The time that the sites stay at the laminar state is surprisingly long and thus the STIT and STI are very robust. Furthermore, the STIT and STI can occur in a wide range of parameter regions; for instance, we can observe STIT and STI in the whole T2S2 SPW.

It can be clearly seen in the figures that the laminar states in the STIT and STI are nothing but the stable T2S2 state, and most of the sites at any given time stay at the T2S2 state while a small portion of the sites are in chaotic motion [see Fig. 7(c)]. The STIT and STI presented in these cases can be briefly explained as follows:

(i) STIT. For even L, there exists a T2S2 attractor. In order to rule out chaotic transient bursts, one must prepare the initial conditions very near the stable state, i.e., in the basin of attraction. The time needed for all the sites to get to the stable states is very long if we take completely random initial conditions. Before all the sites get to the destination, most of the sites are arrested by the laminar state, while a small portion is still in chaotic states. Thus the chaotic sites will act as noise sources and try to kick the laminar sites out of the basin of attraction to turbulence by diffusions. When the noise strength added to a laminar site is big enough in comparison with the basin width $\sigma_{\max}$, this laminar site will burst into turbulence. This is a typical competition process between two phases—the laminar phase and the turbulence phase. The stable attractor tries to arrest all the sites at the laminar state while the unarrested sites tend to kick the rested sites to turbulence by diffusions. The competition maintains a finite time length till all the sites are arrested by the stable state, therefore we observed STIT.

(ii) STI. In the case of odd L there is a mismatch in system size for a stable T2S2 attractor. The STI can be understood as follows. Suppose there is a system with even system size L-1. After the system is attracted by the stable attractor, we add an additional site to the system, and the new site will try to find its stable position. But due to the mismatch in system size, there is always a site

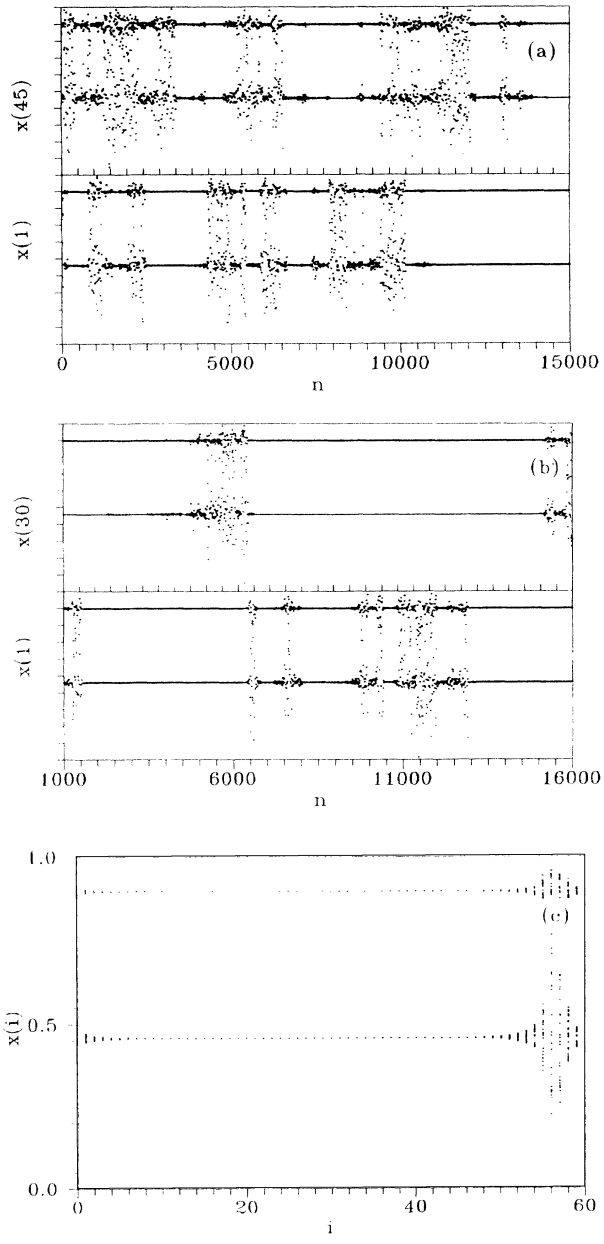

FIG. 7. (a) STIT for $\epsilon=0.15$, $a=4$, and $L=60$. The time evolutions of $x(1)$ and $x(45)$ are shown. (b) STI for $\epsilon=0.15$, $a=4$, and $L=59$. The time evolutions of $x(1)$ and $x(30)$ are shown. (c) The time-space structure for n from 10 000 to 10 050 of the STI in (b).

that cannot find its proper position in the T2S2 state and has to stay at the chaotic motion. This additional site acts as a permanent noise source and thus stimulates and maintains the STI in CML. Actually, this noise source will draw a small number of sites (not only one) away from the laminar state due to the diffusions. So STI instead of STIT is observed.

Obviously, in order to observe robust STI and STIT, one requires that the diffusion constant ϵ should be sufficiently large for creating noise strong enough to kick the laminar sites out of the attracting basin, on the one hand, but sufficiently small to keep the laminar sites to stay at the stable states long enough, on the other hand. The other request for STI and STIT is that the system size should be sufficiently large. In fact, for $L < L_c$ ($L_c \approx 11$ for $\epsilon = 0.15$ and $a = 4$ in our case) no such kinds of robust STIT and STI can be observed. We believe that these kinds of STIT and STI exist very commonly in CML systems or other spatially extended systems.

Although in the T2S4 SPW the stable states have almost the same basin volumes as those of the T2S2 SPW, no such kinds of STI and STIT are observed. The reason is that chaotic noise diffuses so fast due to the strong couplings that the lattice sites are almost not able to stay at the laminar state for sufficiently long periods of time. In Fig. 8, we show the probability distribution for $\epsilon = 0.3$, $a = 4$, and $L = 61$. The data are obtained within 10^5 iterations. It is clearly seen that there are two probability peaks located at $x(i) = 0.4584\ldots$ and $x(i) = 0.8987\ldots$ which are just the two possible states of the T2S4 state. Actually when $L = 4k$, the extremely long transient has the same kind of quasistationary probability distribution. This probability distribution means that the system visits the stable states many more times than the other states, i.e., the system strives to find the stable attractor while the strong diffusions try to kick it out of the stable state. Owing to the large diffusions, the STI phenomenon is not apparent. [Note, if we draw the same probability profile for Fig. 7(b), the two probability peaks should be much sharper than that in Fig. 8.]

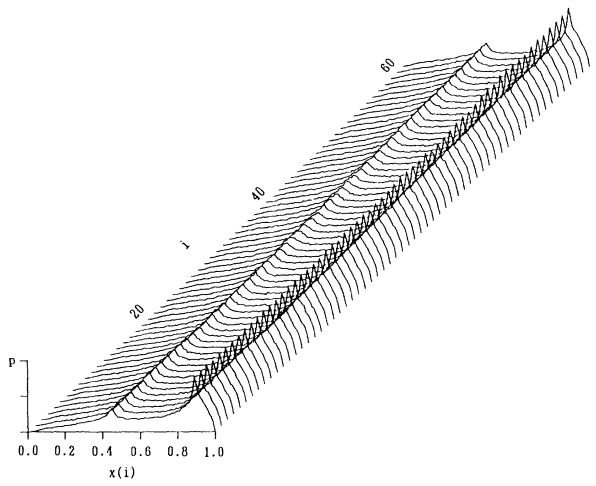

FIG. 8. The probability distribution p versus $x(i)$ and i at $a = 4$, $\epsilon = 0.3$, and $L = 61$. Data are taken within 10^5 iterations.

IV. TRANSIENT STATISTICS

As having been claimed by Cruthfield and Kaneko [5,6], the spatially extended systems exhibit chaotic supertransients. Here we calculate the average transient lengths of the T1S2, T2S2, T2S4, and T2S6 states versus diffusion constant ϵ or system size L. Figure 9 shows the average transient lengths versus ϵ for T1S2, T2S2, and T2S4 states at $L = 4$. We have discussed in Sec. II that the three states have the same Lyapunov spectra and

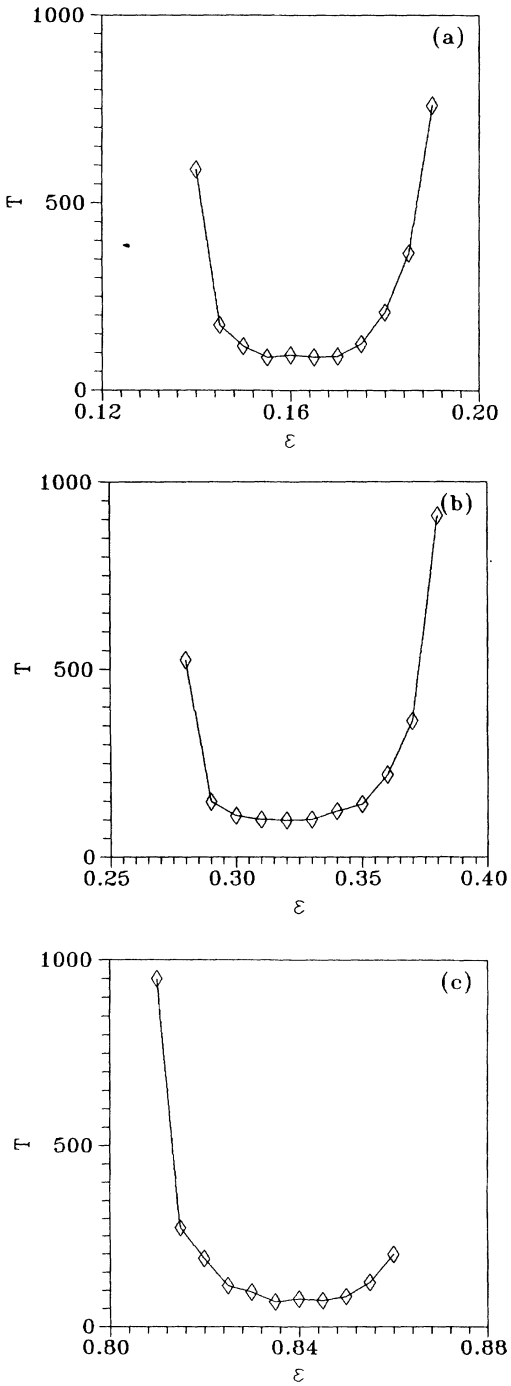

FIG. 9. The average transient lengths versus ϵ for $L = 4$ and $a = 4$. (a) The T2S2 state; (b) the T2S4 state; (c) the T1S2 state.

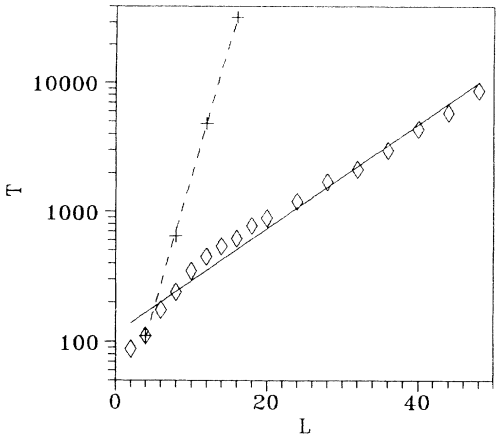

FIG. 10. The average transient lengths versus L at $a=4$ for the T2S2 ($\Diamond$, $\epsilon=0.15$) and T2S4 ($+$, $\epsilon=0.3$) states.

basin width, so it is not difficult to understand that the average transient lengths have similar behaviors versus ϵ in the three regions. Figure 10 shows the average transient lengths of the T2S2 and T2S4 states, which increase exponentially with L versus system size L. The average lengths of these two transients satisfy

$$T=b\exp(cL)\ . \tag{15}$$

For $\epsilon=0.15$, we have $b=114.946$, $c=0.0926$, and for $\epsilon=0.3$, $b=15.6$, and $c=0.47$. Since the basin widths of these attractors are not sensitive to the system sizes, the exponential relation in (15) can be easily understood. (The transient time should be proportional to the basin volume $\sigma_{\max}^{L}$.)

In contrast to those of the T2S2 and T2S4 states, the average transient length of the T2S6 state increases with L in a hyperexponential manner [Fig. 11(a)], which can be fitted as

$$T=b\exp(cL^{d})\ , \tag{16}$$

where $b=392.619$, $c=0.000548$, and $d=3$ for $\epsilon=0.6$ and $a=4$. This hyperexponential feature may be due to the change of the basin widths versus system sizes. Figures 11(b) and 11(c) show the transient processes for $L=12$ and 18, respectively. In contrast to the T2S2 and T2S4 states of which the transition from transient chaos to stable regular motions is very abrupt, for the T2S6 state there is a long nonchaotic transient after the termination of the chaotic transient. The maximum width of the nonchaotic transient can be regarded as proportional to the basin width, which contracts considerably by increasing the system sizes (see Fig. 11). Then the hyperexponential relation in Fig. 11(a) can be intuitively understood.

V. CONTROLLING TRANSIENT CHAOS

Controlling chaos is of current interest. After the first paper by Ott, Grebogi, and Yorke [29], a great number of works have been published [30–36]. But most works focus on low-dimensional systems. To our knowledge, there is no work about controlling chaos on the CML systems reported. Here we report a result of controlling the extremely long chaotic transient to direct the system to the stable attractor in a very short time. The method we have used here is to pin feedbacks to the lattice sites, which is

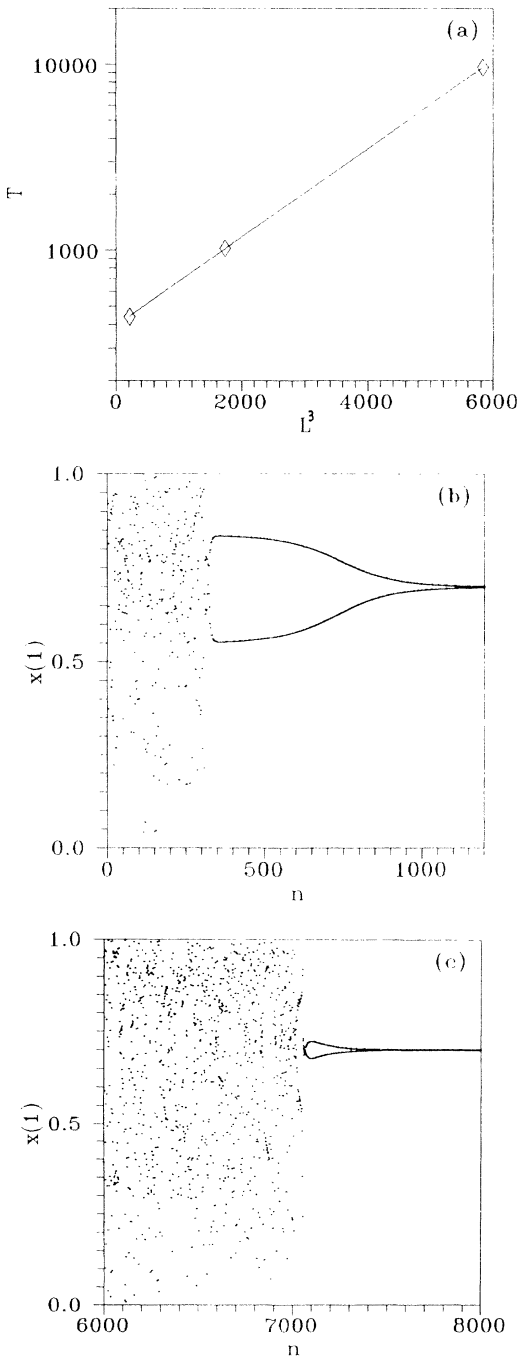

FIG. 11. (a) The average transient length of the T2S6 state versus L for $\epsilon=0.6$ and $a=4$. (b) and (c) The transient evolutions of the T2S6 state for $L=12$ and $L=18$, respectively.

$$x_{n+1}(i)=(1-\epsilon)f(x_n(i)) + \frac{\epsilon}{2}\{f(x_n(i-1))+f(x_n(i+1))\} + g_n\delta(i-Ik)\ , \quad k=1,2,\ldots,L/I \tag{17}$$

where

$$g_n=(1-\epsilon)P_n(i)x_n(i)[x_n(i)-\bar{x}_n(i)] + \frac{\epsilon}{2}\{P_n(i-1)x_n(i-1)[x_n(i-1)-\bar{x}_n(i-1)] + P_n(i+1)x_n(i+1) \times[x_n(i+1)-\bar{x}_n(i+1)]\}\ . \tag{18}$$

I is the distance between pinnings, $\delta(j)=1$ for $j=0$, $\delta(j)=0$ otherwise, and $\bar{x}_n(i)$ is the stable state solution. The reason we use this nonlinear feedback instead of a simple linear one is to prevent the overflows in numerical simulations. Near the stable state the controlling is just the conventional linear negative feedback control [31,32].

As stated in Sec. IV, the transient process for the T2S4 state in a large size system is extremely long; for instance, the average transient length calculated from Eq. (15) is 2.76×10^{13} for $L=60$, and 4.87×10^{25} for $L=120$. For such astronomically long transients, one would have to take one's whole life to wait for the transient to disappear, even if a powerful computer were available. So it is practically important and extremely useful to shorten the supertransient of the spatially extended systems. Here we control the transient for system size $L=60$ by using Eq. (17). If we feed back one site for each 12 sites (the pinning density is very low!), the system evolves quickly to the vicinity of the stable state and shows a time-space regular motion. In Fig. 12 we plot $x_n(i)$ versus i and $x_n(30)$ versus n in the case of controlling; the relaxation length is less than 4000. We have taken various random initial conditions in variable space (0,1), the system always going to the vicinity of the T2S4 state and realizing the asymptotic state of the T2S4 state with few defects. The largest relaxation length we encountered is less than 10^4. We have also controlled the transition of a number of other stable states; our controlling method is found to be very robust and effective and the shortening of the supertransients is really impressive.

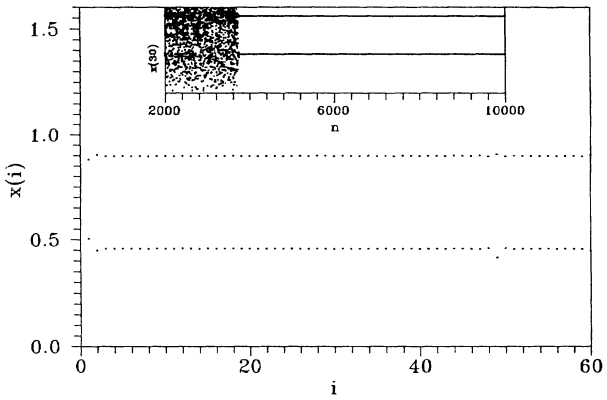

FIG. 12. Time-space structure of the controlled system after 4000 transient iterations, while the small frame plots $x_n(30)$ versus n for n from zero to 10000. We use $P_n(i)=2$ for the sites whose reference states are located at $\bar{x}_n(i)=0.8987\ldots$ and $P_n(i)=1$ for those that $\bar{x}_n(i)=0.4584\ldots$. Pinnings are input at sites $i=1,13,25,37,49$. The initial condition is prepared as completely random numbers.

ACKNOWLEDGMENT

The authors thank Dr. E. J. Ding for useful discussions.

[1] K. Kaneko, Prog. Theor. Phys. **72**, 480 (1984); **74**, 1033 (1985); Physica D **23**, 436 (1986).
[2] J. P. Cruthfield and K. Kaneko, in *Directions in Chaos,* edited by Hao Bai-lin (World Scientific, Singapore, 1987), p. 272.
[3] K. Kaneko, Phys. Lett. A **125**, 25 (1987).
[4] K. Kaneko, Physica D **34**, 1 (1989); D **37**, 60 (1989).
[5] K. Kaneko, Phys. Lett. A **149**, 105 (1990).
[6] J. P. Cruthfield and K. Kaneko, Phys. Rev. Lett. **60**, 2715 (1988).
[7] T. Bohr, G. Grinsten, Yu He, and C. Jayaprakash, Phys. Rev. Lett. **58**, 2155 (1987).
[8] T. Bohr and O. B. Christensen, Phys. Rev. Lett. **63**, 2161 (1989).
[9] P. R. Rasmussen and T. Bohr, Phys. Lett. A **125**, 107 (1987).
[10] J. D. Keeler and J. D. Farmer, Physica D **23**, 413 (1986).
[11] H. Chate and P. Manneville, Europhys. Lett. **6**, 59 (1988); Physica D **32**, 409 (1988); Phys. Rev. A **38**, 4351 (1988); Phys. Rev. Lett. **58**, 112 (1987).
[12] I. Waller and R. Kapral, Phys. Rev. A **30**, 2047 (1984).
[13] R. Kapral, Phys. Rev. A **31**, 3868 (1985).
[14] F. Kaspar and H. G. Schuter, Phys. Rev. A **36**, 842 (1987).
[15] S. Coppersmith, Phys. Rev. A **38**, 375 (1988).
[16] H. Kook, F. H. Ling, and G. Schmidt, Phys. Rev. A **43**, 2700 (1991).
[17] S. Y. Kim and H. Kook, Phys. Rev. A **46**, 4467 (1992).
[18] F. H. Willeboodse, *Chaos, Soliton and Fractals* (Pergamon, New York, 1992), Vol. 2, p. 609.
[19] E. J. Ding and Y. N. Lu, Phys. Lett. A **161**, 357 (1992).
[20] E. J. Ding and Y. N. Lu, Acta Phys. Sin. **1**, 3 (1992).
[21] P. M. Gade and R. E. Amritkar, Phys. Rev. E **47**, 143 (1993).
[22] R. E. Amritkar and P. M. Gade, Phys. Rev. Lett. **70**, 3408 (1993).
[23] P. Grassberger and T. Schreiber, Physica D **50**, 177 (1991).
[24] P. Berge, in *Chaos '87* [Nucl. Phys. B Proc. Suppl. **2**, 247 (1987)].
[25] S. Cilibert and P. Bigazzi, Phys. Rev. Lett. **60**, 286 (1988).
[26] Y. Pomeau and P. Manneville, Commun. Math. Phys. **74**,

189 (1980).
[27] C. Grebogi, E. Ott, and J. A. Yorke, Physica D **7**, 181 (1983).
[28] J. P. Cruthfield, University of California, senior thesis, 1979 (unpublished).
[29] E. Ott, C. Grebogi, and J. A. Yorke, Phys. Rev. Lett. **64**, 1196 (1990).
[30] E. R. Hunt, Phys. Rev. Lett. **66**, 1953 (1991).
[31] K. Pyragas, Phys. Lett. A **170**, 421 (1992).
[32] Qu Zhilin, Hu Gang, and Ma Benkun, Phys. Lett. A **178**, 265 (1993).
[33] W. L. Ditto, S. N. Ranseo, and M. L. Spano, Phys. Rev. Lett. **65**, 3211 (1990).
[34] Z. Gills, C. Iwata, and R. Roy, Phys. Rev. Lett. **69**, 3169 (1992).
[35] C. Reyl, L. Flepp, R. Badii, and E. Brun, Phys. Rev. E **47**, 267 (1993).
[36] D. Auerbach, C. Grebogi, E. Ott, and J. A. Yorke, Phys. Rev. Lett. **69**, 3479 (1992).